Materials Horizons

ROYAL SOCIETY OF CHEMISTRY

COMMUNICATION

View Article Online
View Journal | View Issue

Cite this: *Mater. Horiz.*, 2022, 9, 1518

Received 25th November 2021,
Accepted 15th March 2022

DOI: 10.1039/d1mh01912k

rsc.li/materials-horizons

Performance-oriented multistage design for multi-principal element alloys with low cost yet high efficiency†

Jia Li, ‡[a] Baobin Xie,‡[a] Li Li,‡[a] Bin Liu,[b] Yong Liu,[b] Dmitry Shaysultanov,[c] Qihong Fang,*[a] Nikita Stepanov*[c] and Peter K. Liaw[d]

Multi-principal element alloys (MPEAs) with remarkable performances possess great potential as structural, functional, and smart materials. However, their efficient performance-orientated design in a wide range of compositions and types is an extremely challenging issue, because of properties strongly dependent upon the composition and composition-dominated microstructure. Here, we propose a multistage-design approach integrating machine learning, physical laws and a mathematical model for developing the desired-property MPEAs in a very time-efficient way. Compared to the existing physical model- or machine-learning-assisted material development, the forward-and-inverse problems, including identifying the target property and unearthing the optimal composition, can be tackled with better efficiency and higher accuracy using our proposed avenue, which defeats the one-step component-performance design strategy by multistage-design coupling constraints. Furthermore, we developed a new multi-phase MPEA at the minimal time and cost, whose high strength-ductility synergy exceeded those of its system and subsystem reported so far by searching for the optimal combination of phase fraction and composition. The present work suggests that the property-guided composition and microstructure are precisely tailored through the newly built approach with significant reductions of the development period and cost, which is readily extendable to other multi-principal element materials.

New concepts

The energy shortage and environmental pollution have been great challenges so far for human beings. Here, we report a highly effective, precise, and environmentally friendly material design strategy through a novel machine learning approach integrating the physical laws and a mathematical model, which is successfully applied to the development of complex multi-phase multi-principal element alloys (MPEAs), contributing to the world's carbon neutrality process. Here, a feasible material design avenue is proposed by integrating machine learning, physical laws, and a mathematical model. A newly developed MPEA with a good combination of strength and plasticity exceeding that of its system and subsystems reported so far is then screened and prepared within only two days. It has been demonstrated that the efficiency and economy of the present work are several hundred times higher than those of the existing approach. Most importantly, the present work provides a universal framework for the precise and rapid tailoring of the property-guided composition and microstructure, which further broadens the applicable scope of advanced MPEAs.

Introduction

Obtaining multi-principal element alloys (MPEAs) with excellent mechanical properties through traditional trial-and-error methods is an extremely time- and cost-consuming task, owing to the near-infinite compositional space and its impact on the phase structures.[1–9] Despite the involvement of multi-scale simulation tools and high-throughput technologies,[10–12] the precise design of MPEAs with desired properties is still a challenge due to the complicated process producing complex and uncertain microstructures. Naturally, it is crucial to search for an effective and accurate strategy/approach to predict the structures/properties and design desired-performance MPEA systems. Recently, machine learning has been actively promoted for the development of phase selection, performance prediction, and component screening in MPEAs.[13–15] Nevertheless, the conventional data-driven machine learning models have so far neglected the physical essence of the problems and caused less explainable and poor generalization. Indeed, the existing machine learning models,[16,17] which are still in their

[a] *State Key Laboratory of Advanced Design and Manufacturing for Vehicle Body, College of Mechanical and Vehicle Engineering, Hunan University, Changsha, 410082, P. R. China. E-mail: fangqh1327@hnu.edu.cn*
[b] *State Key Laboratory of Powder Metallurgy, Central South University, Changsha, 410083, P. R. China*
[c] *Laboratory of Bulk Nanostructured Materials, Belgorod State University, Belgorod, 308015, Russia. E-mail: stepanov@bsu.edu.ru*
[d] *Department of Materials Science and Engineering, The University of Tennessee, Knoxville, TN, 37996, USA*

† Electronic supplementary information (ESI) available. See DOI: 10.1039/d1mh01912k

‡ These authors contributed equally to this work.

infancy for computer-aided material design, have been limited to numerically establishing the connection between input and output features. The deep integration of physical cognition and machine learning has not yet been enforced for the development of MPEAs. Here, we provide a universal multistage design framework, by which we successfully design a new multi-phase MPEA. Comparing the tensile properties of this MPEA with its system and subsystems proposed in the literature, it is demonstrated that the present MPEA possesses a superior combination of yield strength and elongation.

To develop multi-phase MPEAs with excellent properties rapidly and accurately, a multistage design method integrating the physical laws, a mathematical model, and machine learning is presented in Fig. 1A. Hence, two core problems should be solved, namely, both the forward problem (FP) avenue (from the composition to desired performance) and the inverse problem (IP) avenue (from the target performance to optimal composition), as shown in Fig. 1B. Here, the multistage strategy has been embedded in the FP and IP avenues, which is composed of two parts, introducing a composition-dependent physics feature space to predict the phase formation and a phase-dependent mathematical model to calculate the yield strength. In order to obtain the target performance, we can screen out the initial composition space and then determine the optimal composition (Fig. 1B). Compared to the results of the one-step strategy, this work can rapidly converge in the desired region, resulting in the reduction of the experimental trial and error, no matter whether in the FP avenue or the IP avenue. Thus, the current novel approach can effectively reduce the development cycle and resource consumption in complicated materials.

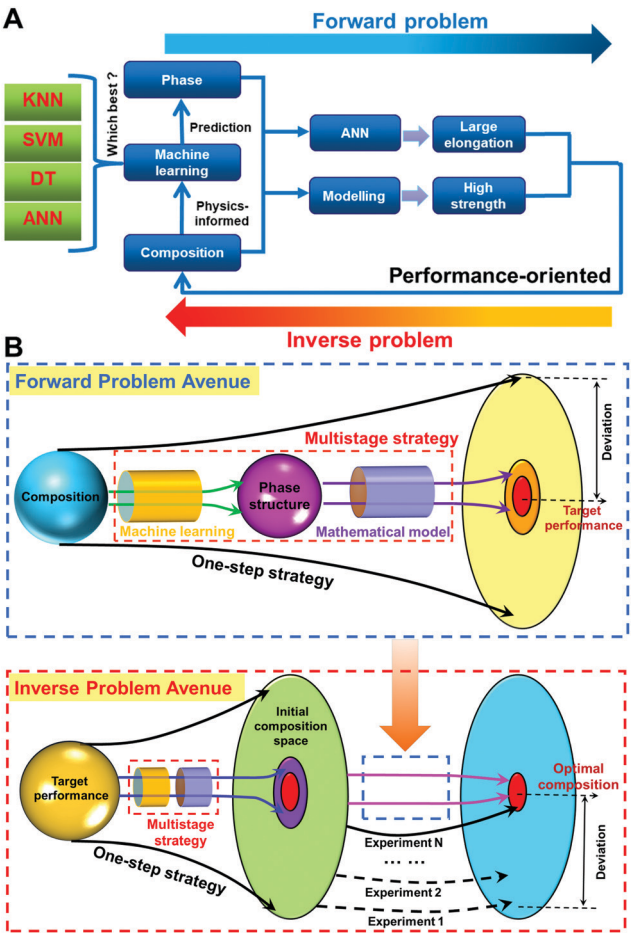

Fig. 1 Strategy of multistage design for performance-oriented precision design. (A) Flowchart of the optimization design in the multi-phase MPEAs with high strength and large elongation. Several common machine learning algorithms, including K-nearest neighbors (KNN), decision tree (DT), support vector machine (SVM), and artificial neural network (ANN), are used to predict the phase selection of MPEAs. Here, the widely studied physics-based features for the phase formation of MPEA are calculated as the initial input features (a detailed description in Table S1, ESI†). (B) The comparisons of the one-step and multistage strategies in the FP and IP avenues. The black arrows represent the process of the one-step strategy. The colored arrows denote the process of the multistage strategy.

Experimental section

Sample preparation

Two alloys with a nominal composition of $Al_{0.63}Co_{0.95}Cr_{0.95}FeMn_{0.74}Ni$ and $Al_{0.55}Co_{0.9}CrFe_{0.95}Mn_{0.8}Ni_{0.8}$ (mole fraction) were produced by vacuum arc melting. High-purity (at least 99.5 weight percent, wt%) powders of the constitutive elements were used as starting materials. The produced ingots had dimensions of $\sim 10 \times 14 \times 50$ mm^3. The ingots were remelted 5 times to ensure the chemical homogeneity. The SEM-EDS analysis showed that the actual chemical composition of the alloy closely corresponded to the nominal one.

Microstructural characterization

The microstructure and phase composition of the alloys in the as-cast condition were studied, using the X-ray diffraction (XRD), scanning electron microscopy (SEM), and transmission electron microscopy (TEM) techniques. The XRD analysis was performed using a RIGAKU diffractometer and Cu Kα radiation. The samples for the SEM observations were prepared by careful mechanical polishing. The SEM investigations were performed employing an FEI Quanta 300 3D and an FEI Nova NanoSEM microscope equipped with back-scattered electron (BSE), energy-dispersive X-ray spectrometry (EDS), and electron back-scattered diffraction (EBSD) detectors. The EBSD phase maps were produced, utilizing TSL OIM software. The samples for TEM analysis were prepared by the conventional twin-jet electro-polishing of mechanically pre-thinned to 100 μm foils, in a mixture of 95% C_2H_5OH and 5% $HClO_4$ at 27 V potential. The TEM investigations were performed, employing a JEOL JEM-2100 microscope equipped with an EDS detector at an accelerating voltage of 200 kV.

Mechanical testing

Tensile mechanical tests were performed, utilizing an Instron 5882 machine. Dog-bone specimens with gauge dimensions of $1.5 \times 3 \times 5$ mm^3 for testing were cut using an electric discharge machine. Prior to testing, the specimens were carefully

mechanically polished. Tensile testing to fracture was carried out at an initial strain rate of 10^{-3} s^{-1}. Elongation to fracture was determined by a VIC-3D system. 3 tests were performed to ensure the consistency of the results.

Mathematical modeling

Mathematical modeling is a very important bridge to relate the fundamental material properties to the macroscopic material behaviors. Here, the fundamental properties (such as composition and elastic moduli) are connected to the specific mechanisms of deformation (such as dislocation slip and phase structure), which then collectively determine the macroscopic properties (such as strength and strain hardening). In MPEAs, the yield strengths can be composed of grain-boundary strengthening and lattice-friction stress. The grain-boundary strengthening in MPEAs is supposed to be similar to that in traditional alloys.[18] However, the lattice-friction stress in MPEAs is significantly different from that in traditional alloys, owing to their intrinsic multi-principal characteristics. Here, we utilize the lattice-distortion-introduced stress originating from the atomic difference between various multi-principal elements in MPEAs to replace the sum of the solid-solution strengthening and lattice-friction stress in traditional alloys, owing to the fact that there is no definite distinction between the solute and solution in MPEAs. It is noted that the present model contains no fitting parameters. The computed inputs are the compositions and phase structures of the MPEAs, where the former is the inherent feature of materials, and the latter can be obtained by the machine learning approach. The detailed calculation description of yield strength is provided in Supplementary Text S1 (ESI†) ''Yield strength of MPEAs''. Here, the proposed mathematical model can directly calculate the yield strength of single-phase MPEAs. For the dual-phase MPEAs, their yield strength is predicted through the mixing theory, which needs the phase volume fraction calculated based on the constructed ''composition-FCC/BCC volume fraction'' model by machine learning (Supplementary Text S2, ESI†).

Data collection

The initial ''composition-phase structure'' data set is built by collecting the available experimental results in the previous literature (a detailed alloy composition and the corresponding source in Data S1, ESI†), including 325 entries with some common MPEA systems, such as Al–Fe–Co–Cr–Ni–Mn, Co–Cr–Fe–Ni, and Mo–Nb–Ta–V–Zr. Furthermore, considering that these process parameters have a significant influence on the microstructure and properties, the MPEAs collected in the initial data set were all prepared by arc melting to prevent measurement differences. The data set includes three MPEA phase structures (BCC, BCC + FCC, and FCC). Because there are few HCP MPEAs so far, the HCP MPEAs are excluded to avoid unbalanced data distribution. In addition, to ensure the reliability of the data set and improve the accuracy and efficiency of the machine learning model, data cleaning is a critical step before using machine learning algorithms. The basic guideline is that each MPEA composition corresponds to a unique phase and each item appears only once. Besides, all of the entries with the same composition yet different phase structures induced by the variation of the process parameters need to be excluded because the accuracy of these data cannot be figured out. Meanwhile, some obvious outlier entries are removed by observing the distribution of the input features (see the detailed description of the input features in the Data analysis section). After data cleaning, the final data set for phase prediction is composed of 266 entries with 103 BCC, 61 FCC and 102 BCC + FCC phases (Data S2, ESI†).

Machine learning algorithm

The performance of the four machine learning algorithms, including the KNN algorithm, DT algorithm, SVM algorithm, and ANN algorithm, are evaluated in the current work. In order to protect against the over-fitting issue when using machine learning algorithms, the five-folds cross-validation method is used for the KNN, DT, and SVM algorithms while an early-stopping strategy is adopted for the ANN algorithm. The descriptions of these machine learning algorithms, five-folds cross-validation method and early-stopping strategy are elaborated in Supplementary Text S1 (ESI†) ''Machine learning algorithm''.

Results and discussion

Data analysis

Before the implementation of the machine learning algorithms, it is critical to determine the appropriate descriptors as the input features. Apparently, it is unreasonable to use the elements and corresponding composition fraction as descriptors because of the unpredictable dimensional disaster and excessive computation. Luckily, Hume-Rothery rules[19] denote that some physical features, such as the valence electron concentration (VEC), mixing entropy (ΔS_{mix}), mixing enthalpy (ΔH_{mix}), atomic-size difference (δ) and electronegativity difference ($\Delta\chi$), are closely related to the phase formation of MPEAs. Based on the previous work, some other important physics features, such as thermodynamics features[20] (average melting temperature T_m, and thermal stability parameters Ω), atomic features[21] (γ), physical properties (elastic modulus E, bulk modulus B, and alloy density ρ) and hybrid features[22] (λ), are adopted as the input features to expand the parameter space. The detailed description and formula of the twelve physical features are presented in Table S1 (ESI†). Subsequently, the values of the features are normalized to (0,1): (i) each individual feature has the same numerical scale; (ii) all features are treated equally. Furthermore, the *t*-stochastic neighbor embedding (t-SNE) method[23] is used to investigate the feature distribution of the whole sample in two dimensions, as shown in Fig. 2 (the detailed data corresponding to each MPEA in Data S3, ESI†). The original data distribution can be presented in Fig. S1 (ESI†). There are two advantages of choosing the t-SNE method for data analysis: (i) converting the high dimension data into low dimension space makes the data distribution be better

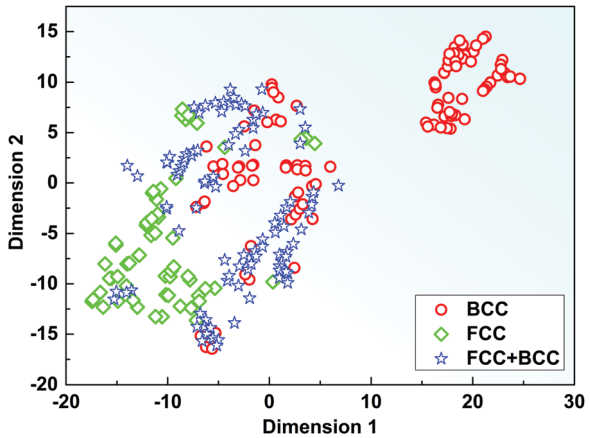

Fig. 2 Feature distribution of the 266 samples in two-dimensional spaces *via* t-SNE.

visualized, and each axis does not need to be given a clear physical meaning; (ii) original information of the high dimensional feature space can be maintained. Here, there are some BCC alloys far away from other materials (the top right of Fig. 2), which are mainly refractory MPEAs, such as Nb–Ta–Ti–V, Hf–Nb–Ta–Zr, and Mo–Nb–Ta–Ti–Zr systems. For the MPEAs lacking the refractory elements, such as Cr–Co–Fe–Ni and Cu–Al–Cr–Co–Fe–Ni systems, they mainly locate at the left region of Fig. 2. Furthermore, although the distributions of the BCC and FCC phases are obviously separated, the samples of the BCC + FCC phases are significantly entangled with them. This trend indicates that the feature information of them in origin high dimension space is similar. Therefore, using empirical rules to identify the phase selection is difficult. Accordingly, in this work, a machine learning model with high efficiency and accuracy is developed to search for the nonlinear mapping that distinguishes the feature distribution of various phases. Moreover, in view of the small data size, the current machine learning model could predict accurately the phases of MPEAs, which are limited in the initial data set.

Phase prediction

In order to obtain the optimal features of phase predictions, removing less important features can perform more reliably in classification tasks while decreasing the size of the machine learning models. Here, a feature engineering scheme combined with correlation analysis with physical knowledge is used to search for an optimal number of features and reduce the size of the feature space. Fig. 3A shows the Pearson correlation coefficient[24] matrices for every possible input feature pair obtained from 12 features. Less than 10% of features have absolute values of correlation coefficients larger than 0.8 (Fig. 3A), confirming the relatively small redundancy. Furthermore, the physics information of the features is mined to reduce the size of the feature space to an optimal number of the correlated features (Fig. 3B). Thus, the original 12 features are converted to the 9 features resulting in a smaller feature space in the final classification process. Importantly, a more robust machine learning model can be generated by decreasing the number of features.

To select the best machine learning algorithm for phase predictions, various machine learning models are evaluated (performance of the machine learning algorithm in Supplementary Text S3, ESI†). Here, the accuracy values of KNN, SVM, and DT are the average of five testing results, and the accuracy of ANN represents the average of the training, validation and testing data set, *i.e.*, the average of the entire data set. Fig. 3C indicates the comparison of the accuracy, and ANN is of potential interest for prediction performance. Meanwhile, the proposed feature engineering scheme significantly enhances the efficiency of the model without sacrificing the prediction accuracy. Moreover, for discovering the criterion on how to confirm the phase selection, the sensitivity measures for the BCC, BCC + FCC, and FCC structures are calculated, respectively. The result of the trained ANN model for the sensitivity measure of the feature (Fig. 3D) illustrates that the weight coefficient of the VEC to decide the phase structure gradually declines, accompanied by the increase of the weight coefficient of the mixing enthalpy, which breaks the traditional rule of VEC acting as only the high impact feature.[25,26] Hence, the formation mechanism of multi-phases is extremely complex, and this result gives avenues towards the multi-mechanism criterion that beats the single rule for precise structural design.

Yield strength of multi-phase MPEA

To accelerate the development of the complex materials, it is very common to construct the correlation among the composition, microstructure, and mechanical performance.[18] Therefore, a mathematical model is established to predict the yielding strength of the MPEA. Simultaneously, the elongation of MPEA is obtained using the machine learning approach due to the lack of an accurate prediction model for the ductility (Supplementary Text S4, ESI†).

We have carefully curated literature data on the yield strengths of a range of MPEAs with various phase structures, including the FCC, BCC, and FCC + BCC phases. The yield strengths of the BCC and FCC MPEAs are significantly different, in which those of most FCC MPEAs is less than 400 MPa, and those of most BCC MPEAs is larger than 900 MPa (Fig. 4A). Then, the predicted strength data are compared to the experimental data, and there is a fairly good agreement between the prediction and experiment (Fig. 4A). The further statistics indicate that the computed results with the deviation less than 3% account for 28.3%, with the deviation larger than 3% and less than 10% represent 34%, and with the deviation larger than 10% and less than 20% denote 30.2%. Specifically, only 7.5% of the prediction data has a deviation larger than 20%. Furthermore, it has been confirmed that the prediction accuracy of this model is superior to other typical models out of many potential candidates (Fig. 4B). This developed mathematical model integrating machine learning would be efficiently used as constraints to predict properties of hypothetical MPEAs when applied to data-driven materials. These results illustrate that this mathematical model possesses excellent quantitative

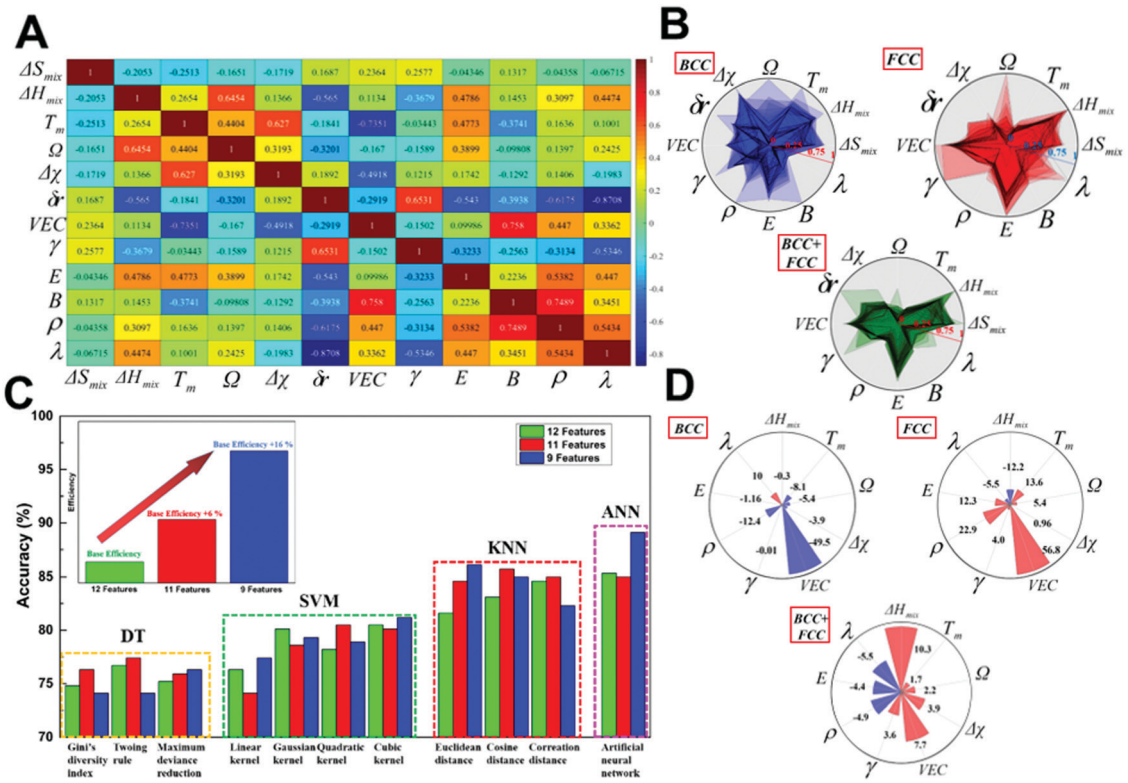

Fig. 3 The correlations between the input physical features and prediction accuracy of machine learning models. (A) Pearson correlation coefficients for 12 features. The value in each grid represents the correlation coefficient between two features, 1 (−1) denotes the completely positive (negative) correlation, and the colour intensity reflects the magnitude of the correlation coefficient. (B) Polar charts for the distributed characteristics of 12 features in the BCC, BCC + FCC, and FCC phases, respectively. An area with a higher color intensity indicates the average distribution shape of the phase structure in the feature space. (C) Comparing the prediction performance using various machine learning algorithms with different training parameters. The green pillar represents the machine learning model built with 12 features, the red pillar denotes 11 features, and the blue pillar means 9 features. Based on the efficiency of the models with 12 features as benchmark efficiency, the efficiency of the model improves 16%, using the proposed feature engineering scheme. (D) The sensitivity measures with 9 features for the BCC, BCC + FCC, and FCC structures *via* a Nightingale rose diagram. The red (blue) color represents that the sensitivity measure of the feature is positive (negative). The radius of the sector denotes the value of the magnitude of the sensitivity measure.

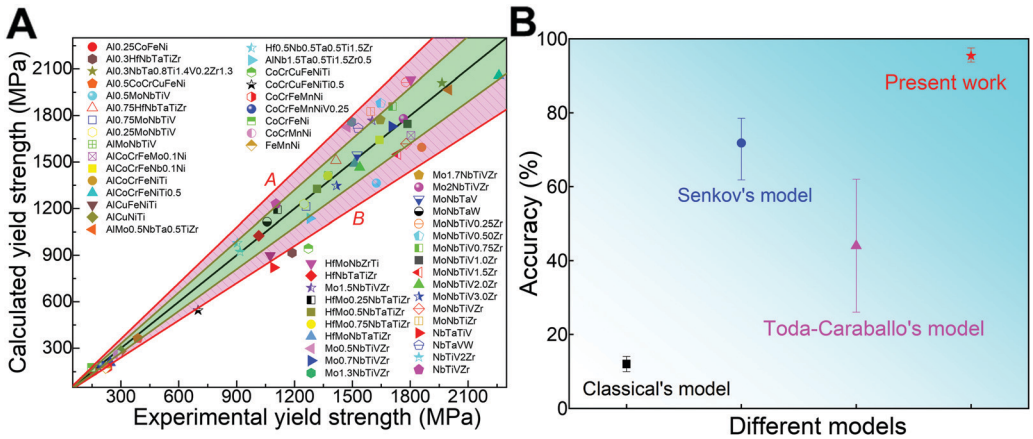

Fig. 4 The strength prediction and its accuracy. (A) The deviation relationship of the yield stress between the experimental and calculated results for various MPEAs (Data S4, ESI†). The black line denotes that the calculated result coincides perfectly with the experimental data. The light green area indicates that the deviation is smaller than 10%. The pink area represents that the deviation is larger than 10% but smaller than 20%, and the A and B areas denote that the deviation is larger than 20%. (B) The comparison of the prediction accuracy between the proposed model and other typical models, which is counted from various samples, including the representative FCC CrCoFeNiMn, BCC TiNbTaZrHf, and dual-phase $Al_{0.5}$CrCoFeNiMn MPEAs. The experimental data sources and modeling predictions have been provided in Table S2, ESI.†

predictive capability and universal applicability to compute the yield strengths of MPEAs. Thus, the present model can be integrated into the machine learning approach, for a further selection of MPEAs with outstanding properties by considering various aspects: multi-component, multi-phase, and multiple-strengthening mechanisms.

Application of the multistage design strategy

The most important contribution of the current multistage design approach is to deduce the accurate element composition and phase structure. Here, the classical FeCoCrNiMn (Cantor) system is the basic principle component, and then the introduction of the Al element produces multi-phase MPEAs.[27] Meanwhile, the new $Al_{0.63}Co_{0.95}Cr_{0.95}FeMn_{0.74}Ni$ MPEA, having a good combination of strength and plasticity, has been predicted through the IP avenue in Fig. 1B (Supplementary Text S2, ESI† "Prediction of the optimal composition in the Al–Fe–Co–Cr–Ni–Mn system"). To check the validity of the predictions, this alloy is prepared by arc melting. From the XRD pattern of Fig. 5A, the intensity of the peaks from the FCC and BCC phases is similar, and the alloy is composed of both phases with the lattice parameters of 0.361 and 0.289 nm, respectively. To identify the crystal structures of the constitutive phases, the EBSD analysis is performed (Fig. 5B), where the estimated volume fractions of the FCC and BCC phases are 72% and 28%, respectively. The TEM studies are performed to analyze the structure of the alloy at a nanoscale (Fig. 5C), where the existence of FCC and BCC phases is confirmed by corresponding selected area electron diffraction patterns (#1, #2, and #3 in Fig. 5C). This trend agrees reasonably well with the available literature data.[27,28] Finally, the chemical compositions of the constitutive phases measured by the TEM-based EDS analysis are presented in Table S3 (ESI†). The FCC phase has a composition close to the nominal one, and the BCC phase is enriched with Cr and Fe and depleted of the rest of the elements. The tensile stress–strain curve in Fig. 5D shows a high yield strength of 880 MPa, the ultimate tensile strength of 1,235 MPa, and the elongation of 12.3%. Furthermore, the experimental results suggest that the new MPEA proposed in the current work thoroughly defeats the properties of its existing system/subsystems and other MPEAs reported in previous literature,[27] as presented in Fig. 5E. The experimental strength and elongation are also located in the range of screening criteria (strength $>$ 800 MPa and elongation $>$ 10%, the detailed explanation is mentioned in Supplementary Text S2, ESI†). Therefore, a new alloy system with excellent mechanical properties can be designed, which only takes two days, including the prediction, preparation, characterization, and performance test. These results imply the key role of our novel avenue in designing high-performance MPEAs. Moreover, in order to further demonstrate the validity comprehensively of the proposed multistage-design approach, the $Al_{0.55}Co_{0.9}CrFe_{0.95}Mn_{0.8}Ni_{0.8}$ MPEA with suboptimum properties has been re-selected and re-prepared. The detailed description is presented in Supplementary Text S5 (ESI†).

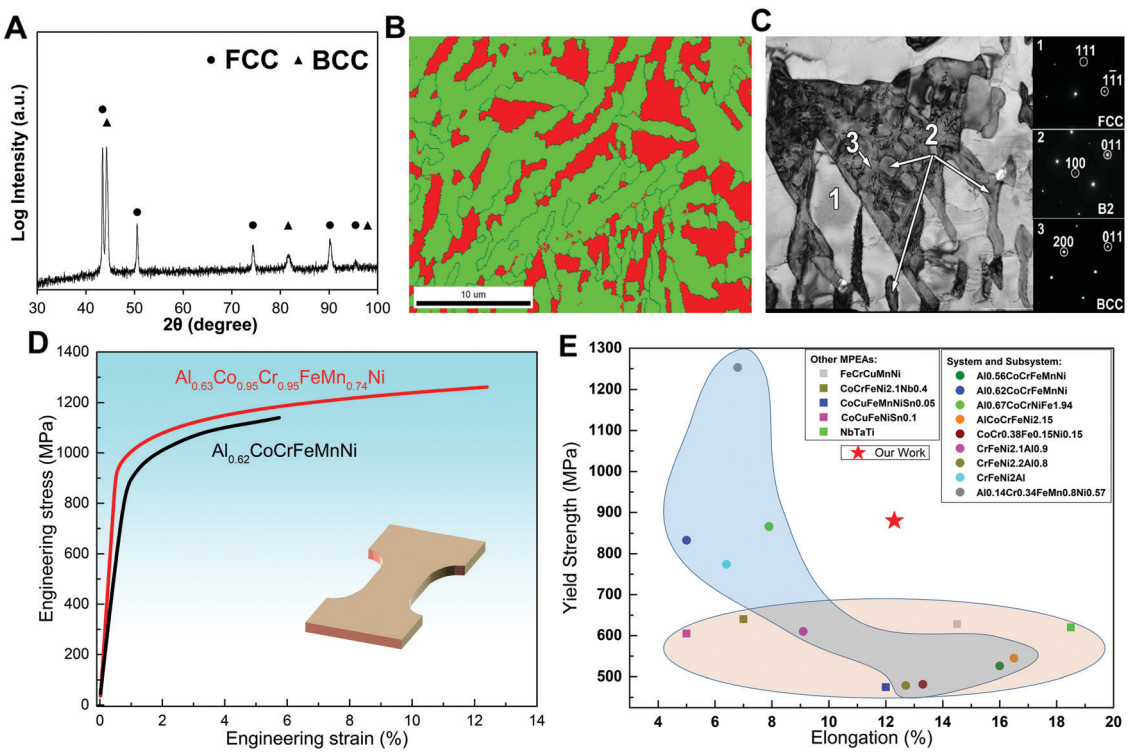

Fig. 5 Results of the validation experiment. (A) Structural and mechanical properties of the as-cast $Al_{0.63}Co_{0.95}Cr_{0.95}FeMn_{0.74}Ni$ MPEA: XRD pattern. (B) EBSD phase map (the green color depicts the FCC phase, and the red denotes the BCC one). (C) TEM bright-field image with selected area electron diffraction patterns. (D) Tensile stress–strain curve. (E) Ashby plot of elongation *versus* the yield strength of the Al–Co–Cr–Fe–Ni–Mn system, and other MPEA systems (Table S4, ESI†).

Comparison of the design methods

The existing one-step strategy used in designing MPEAs usually attempts to directly establish the relationship from the composition to performance.[29–32] However, this mode neglects the complex phase structure dependent upon composition, thus causing a significant deviation between the computed and target performance. For example, using a one-step strategy, the AlCoCrCuFeNi MPEA with desired performance was prepared successfully at the expense of several series of experimental feedbacks, due to the existence of phase transformation with the variations in Al and Cu contents.[29] Moreover, the precipitation strengthened copper alloys with high properties were also obtained by the one-step strategy but were verified by 12 experiments owing to the lack of microstructure-to-performance correlation.[30] The present work introduces the composition-dominated phase structure as the intermediary and thus realizes the multistage strategy, integrating physics-guided machine learning to predict phase formation, and a microstructure-controlled mathematical model to calculate the yield strength. Firstly, a ''physics-feature-space'' is constructed to describe the phase formation of MPEAs and embed it into machine learning. Compared to the case for the composition as descriptors, the physical feature-constrained machine learning model not only contributes to accurately revealing a general criterion of phase formation (Fig. 3D) but also makes the model explainable and universal. The classical feature engineering method based on the Pearson coefficient for the phase prediction of MPEA has been fully reported.[24] Nevertheless, this feature analysis method is one-sided because only numerical correlations between features are assessed, causing some potential redundant features to remain. Therefore, the proposed feature engineering method that comprehensively considers the Pearson coefficient and physical features (Fig. 3B) becomes more reasonable, effectively improving the accuracy and efficiency of the machine learning model (Fig. 3C). The developed mathematical model considers the extensive strengthening mechanisms, such as the grain boundary strengthening, phase transformation strengthening, and solid solution strengthening.[33,34] Hence, the current model is universal for multiphase MPEAs, whose accuracy in the predicted strength is up to 90% and overmatches that of other existing models (Fig. 4). The robust machine learning and mathematical models are the intrinsic reason for the accuracy of this novel approach in the FP avenue. Compared to the one-step strategy, the multistage strategy significantly reduces the initial composition space in the IP avenue. Subsequently, the FP avenue is employed to compute the performance of the initial composition space and screen out the optimal composition based on the optimal performance, avoiding a lot of experimental trial and errors and obtaining low cost yet high efficiency using the multistage design strategy.

As is well-known, the high strength of the alloy most likely stems from the multiphase microstructure (Fig. 5E). For the Al–Co–Cr–Fe–Ni–Mn system, the combination of Al and Ni tends to form the BCC phase because of the high formation enthalpy.[29] With increasing the Al content, the MPEAs transform from the FCC phase to the BCC + B2 phase. Thus, the multiphase enabling strength-plasticity synergy is developed, owing to the following reason: the FCC matrix provides a reasonable elongation and good strain-hardening capacity, and the BCC and B2 phases acted as hard reinforcement and generate strong back stresses in the softer FCC phase. Our multistage strategy can capture this rule hidden, guiding the experimental exploration of the multi-phase MPEAs that go beyond the limitations of the conventional alloy performance. With respect to the cycle of the development for alloys, a comparison with the major technologies is presented in Fig. 6. The traditional experiments are the most time- and cost-consuming, due to lots of trials and errors. The high-throughput, theoretical model and simulation-assisted experiments enhance efficiency (or reduce cost) to a certain extent. This is derived from the wide composition range space and its induced uncertainty of the microstructure. The existing design strategy combining machine learning and experiments still requires some trials as feedback. Here, the cost and efficiency of the proposed approach virtually exceed those of previous material design technologies, providing a new avenue to simultaneously achieve rapid and accurate material design.

In the present work, we have proposed a multistage design approach integrating machine learning, physical laws, and a mathematical model to achieve the rapid design of the multiphase MPEA. Based on the proposed strategy, a new multiphase MPEA is developed in a very short amount of time and low consumption. Importantly, the comprehensive mechanical properties outperform its system and subsystems reported previously, which achieves accurate design for MPEAs with high strength and ductility. It is believed that the present work provides a fundamental framework to guide the design of advanced materials through a means of high efficiency and low cost, helpful for reducing resource consumption.

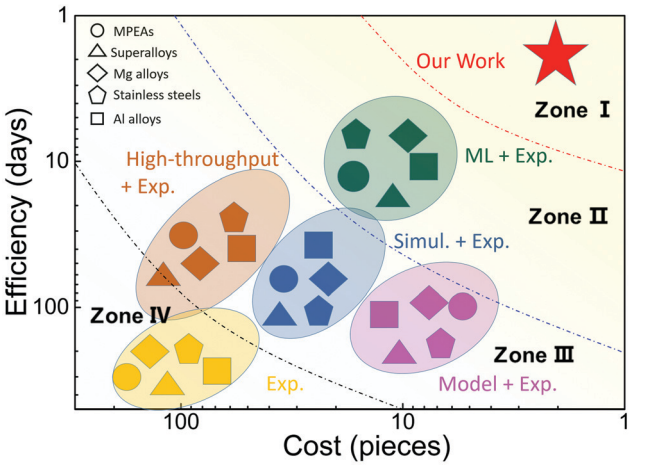

Fig. 6 Advantages of the method. Ashby map showing efficiency as a function of cost and time in relation to the potential material design technologies (Table S5, ESI†). Zones I–IV represent a deteriorating combination of efficiency and cost.

Data and code availability

All data needed to evaluate the conclusions are present in the paper and/or the ESI.† The code will be made available upon request.

Author contributions

Q. H. F., N. S., and P. K. L. were responsible for the supervision, analysis, editing, and funding acquisition. J. L., B. B. X. and L. L. carried out the machine learning and theoretical calculations. D. S. performed the experiments. B. L. and Y. L. analyzed the data. All authors discussed the results and wrote the manuscript.

Conflicts of interest

The authors declare that they have no competing interests.

Acknowledgements

The authors would like to deeply appreciate the National Natural Science Foundation of China (12172123, 12072109 and 51871092). P. K. Liaw very much appreciates the support from the National Science Foundation (DMR-1611180 and 1809640).

Notes and references

1 E. P. George, D. Raabe and R. O. Ritchie, *Nat. Rev. Mater.*, 2019, **4**, 515–534.
2 C. Oses, C. Toher and S. Curtarolo, *Nat. Rev. Mater.*, 2020, **5**, 295–309.
3 T. Yang, Y. L. Zhao, Y. Tong, Z. B. Jiao, J. Wei, J. X. Cai, X. D. Han, D. Chen, A. Hu and J. J. Kai, *Science*, 2018, **362**, 933–937.
4 Z. Lei, X. Liu, Y. Wu, H. Wang, S. Jiang, S. Wang, X. Hui, Y. Wu, B. Gault and P. Kontis, *Nature*, 2018, **563**, 546–550.
5 Y. Yao, Z. Huang, P. Xie, S. D. Lacey, R. J. Jacob, H. Xie, F. Chen, A. Nie, T. Pu and M. Rehwoldt, *Science*, 2018, **359**, 1489–1494.
6 S. Wei, S. J. Kim, J. Kang, Y. Zhang, Y. Zhang, T. Furuhara, E. S. Park and C. C. Tasan, *Nat. Mater.*, 2020, **19**, 1175–1181.
7 Q. Ding, Y. Zhang, X. Chen, X. Fu, D. Chen, S. Chen, L. Gu, F. Wei, H. Bei and Y. Gao, *Nature*, 2019, **574**, 223–227.
8 C. Lee, G. Kim, Y. Chou, B. L. Musicó, M. C. Gao, K. An, G. Song, Y.-C. Chou, V. Keppens and W. Chen, *Sci. Adv.*, 2020, **6**, eaaz4748.
9 D. B. Miracle and O. N. Senkov, *Acta Mater.*, 2017, **122**, 448–511.
10 M.-X. Li, S.-F. Zhao, Z. Lu, A. Hirata, P. Wen, H.-Y. Bai, M. Chen, J. Schroers, Y. Liu and W.-H. Wang, *Nature*, 2019, **569**, 99–103.
11 R. Singh, A. Sharma, P. Singh, G. Balasubramanian and D. D. Johnson, *Nat. Comput. Sci.*, 2021, **1**, 54–61.
12 Z. Wu, R. Ahmad, B. Yin, S. Sandlöbes and W. A. Curtin, *Science*, 2018, **359**, 447–452.
13 Z. Zhou, Y. Zhou, Q. He, Z. Ding, F. Li and Y. Yang, *npj Comput. Mater.*, 2019, **5**, 1–9.
14 J. M. Rickman, H. M. Chan, M. P. Harmer, J. A. Smeltzer, C. J. Marvel, A. Roy and G. Balasubramanian, *Nat. Commun.*, 2019, **10**, 1–10.
15 L. J. Santodonato, P. K. Liaw, R. R. Unocic, H. Bei and J. R. Morris, *Nat. Commun.*, 2018, **9**, 1–10.
16 G. E. Karniadakis, I. G. Kevrekidis, L. Lu, P. Perdikaris, S. Wang and L. Yang, *Nat. Rev. Phys.*, 2021, **3**, 422–440.
17 J. L. Lansford and D. G. Vlachos, *Nat. Commun.*, 2020, **11**, 1–12.
18 J. Fish, G. J. Wagner and S. Keten, *Nat. Mater.*, 2021, **20**, 774–786.
19 Y. Zhang, Y. J. Zhou, J. P. Lin, G. L. Chen and P. K. Liaw, *Adv. Eng. Mater.*, 2008, **10**, 534–538.
20 X. Yang and Y. Zhang, *Mater. Chem. Phys.*, 2012, **132**, 233–238.
21 Z. Wang, Y. Huang, Y. Yang, J. Wang and C. T. Liu, *Scr. Mater.*, 2015, **94**, 28–31.
22 A. K. Singh, N. Kumar, A. Dwivedi and A. Subramaniam, *Intermetallics*, 2014, **53**, 112–119.
23 S. Y. Lee, S. Byeon, H. S. Kim, H. Jin and S. Lee, *Mater. Des.*, 2021, **197**, 109260.
24 Z. Pei, J. Yin, J. A. Hawk, D. E. Alman and M. C. Gao, *npj Comput. Mater.*, 2020, **6**, 1–8.
25 R. Chen, G. Qin, H. Zheng, L. Wang, Y. Su, Y. Chiu, H. Ding, J. Guo and H. Fu, *Acta Mater.*, 2018, **144**, 129–137.
26 V. Chaudhary, R. Chaudhary, R. Banerjee and R. V. Ramanujan, *Mater. Today*, 2021, **49**, 231–252.
27 J. Y. He, W. H. Liu, H. Wang, Y. Wu, X. J. Liu, T. G. Nieh and Z. P. Lu, *Acta Mater.*, 2014, **62**, 105–113.
28 N. D. Stepanov, D. G. Shaysultanov, R. S. Chernichenko, M. A. Tikhonovsky and S. V. Zherebtsov, *J. Alloys Compd.*, 2019, **770**, 194–203.
29 C. Wen, Y. Zhang, C. Wang, D. Xue, Y. Bai, S. Antonov, L. Dai, T. Lookman and Y. Su, *Acta Mater.*, 2019, **170**, 109–117.
30 H. Zhang, H. Fu, S. Zhu, W. Yong and J. Xie, *Acta Mater.*, 2021, **215**, 117118.
31 W. Wan, X. Jiang, S. Tian, P. Liu, D. Dang, Y. Su, T. Lookman and J. Xie, *npj Comput. Mater.*, 2022, **8**, 1–12.
32 B. Xiong, X. Zhao, Y. Hu, H. Huang, Y. Liu and Y. Su, *Mater. Des.*, 2021, **210**, 110037.
33 B. Yin, S. Yoshida, N. Tsuji and W. A. Curtin, *Nat. Commun.*, 2020, **11**, 1–7.
34 C. Varvenne, A. Luque and W. A. Curtin, *Acta Mater.*, 2016, **118**, 164–176.